AA241X Problem Set 3

Apoorva Sharma, Justin Schneider, Miao Zhang, Victoria M Dax, Zhe Zhang and Zhengyu Huang

June 6, 2017

Contents

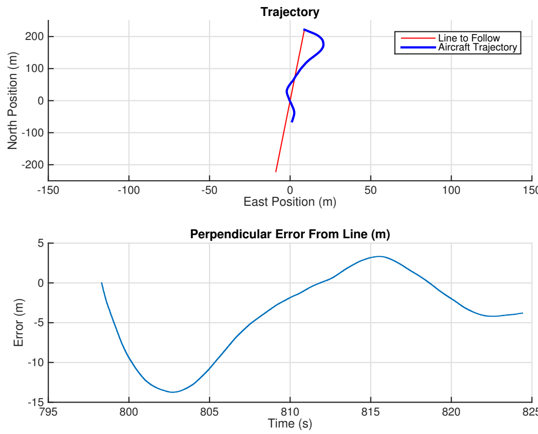

(a) Trajectory and Perpendicular Error

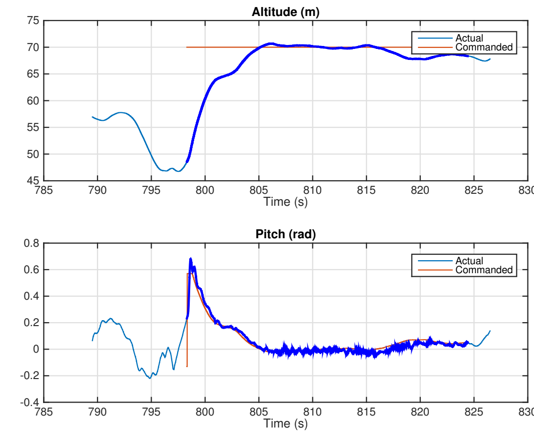

(b) Altitude and Pitch Histories

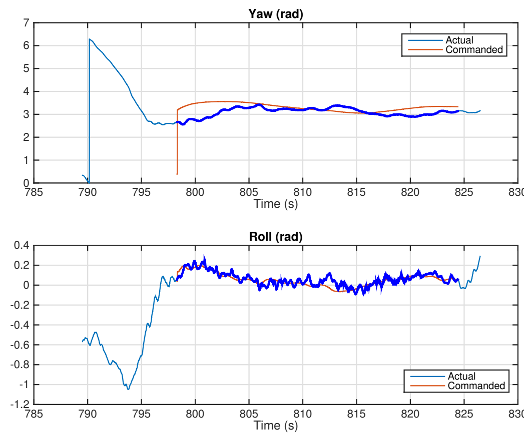

(c) Yaw and Roll Histories

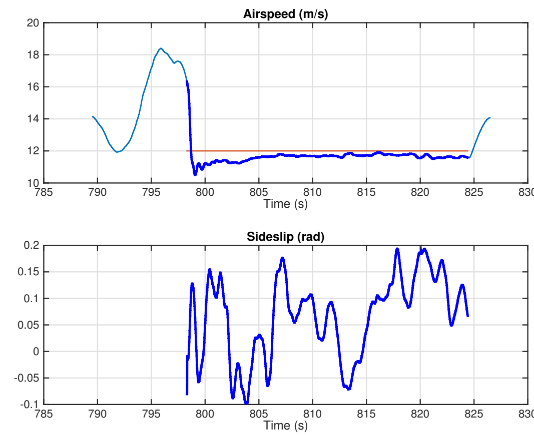

(d) Velocity and Sideslip Histories

Figure 1: Line acquisition and tracking with the Bixler aircraft. Altitude is tracked well, however, the perpendicular error dynamics are slow and have overshoot, indicating that the gains can be better tuned.

I Acquisition of a line

As a first step towards full waypoint path following, we first implemented a controller to have the aircraft autonomously follow a defined line in space. This line following controller is the same controller that was implemented and tested in simulation for problem set 2. The controller to follow the line uses the perpendicular error between the plane and the desired path to follow to compute the desired course to command to the lower level course hold loop.

We define the 2D line to follow with a starting point $\mathbf{q}$ and a heading χ_q. Let $\mathbf{p}$ be the current position of the plane. Given these definitions, we can compute perpendicular error and then the course to command χ^c using the process below.

$$\begin{aligned}\mathbf{e} &= \mathbf{p} - \mathbf{q} \\ e_\perp &= \mathbf{e}_e \cos(\chi_q) - \mathbf{e}_n \sin(\chi_q) \\ \chi^c &= \chi_q - \chi_\infty \frac{2}{\pi} \arctan(k_{\text{path}} e_\perp)\end{aligned}$$

Note that there are two parameters of this controller: χ_∞, the angle at which to approach the line if the perpendicular error is large, and k_{path} which determines the sensitivity of the commanded course on the perpendicular error.

We did initial testing of this controller with the Bixler, using $\chi_\infty = \pi/5$ and $k_{\text{path}} = 0.05$. The resulting performance, shown in Figure 1, shows that these choices were too conservative - the dynamics of the perpendicular error were much slower than desired, and there was significant overshoot. We updated these parameters when testing transitions between lines and waypoint tracking, but we did not collect data on line acquisition alone with better tuned gains.

II Transition between lines

In this section, we will show two flight paths to demonstrate the capability to follow specified paths in the air. From Figures 2 and 4, we can see that the Bixler3 is supposed to fly to the green circle (target 0), the red circle (target 1), the blue circle (target 2), the purple circle (target 3) and the yellow circle (target 4). The simple straight line path is shown in the red lines. The target circles have radius 10m. The plane is controlled to acquire the line connecting the previous waypoint to the next waypoint. Upon reaching within the radius of the target, the target waypoint is updated, so the line to acquire switches to the next segment. We can see that acquiring the line takes quite a long time with the tested control parameters, and thus the Bixler often does not fly within the 10m radius of the waypoint. Specifically, the course controller has a slow response, which leads to the slow response and overshoot of the line following controller. Since the commanded roll is not saturating much, even for near 180 degree turns, we will be able to increase the proportional gain on the course controller more to achieve tighter line following and line switching.

The altitude of these target points are set to be {60.0m ,50m, 60.0m ,50.0m ,60.0m} and the velocity is set to be 17m/s. From the altitude and velocity plot in Fig (5) (5) , the controller can successfully switch the altitude from 50m to 60m to 50m etc. The controller holds the velocity around 17m/s with some offset. The offset is hypothesized to be due to poor modeling of the trim throttle value for the given speed.

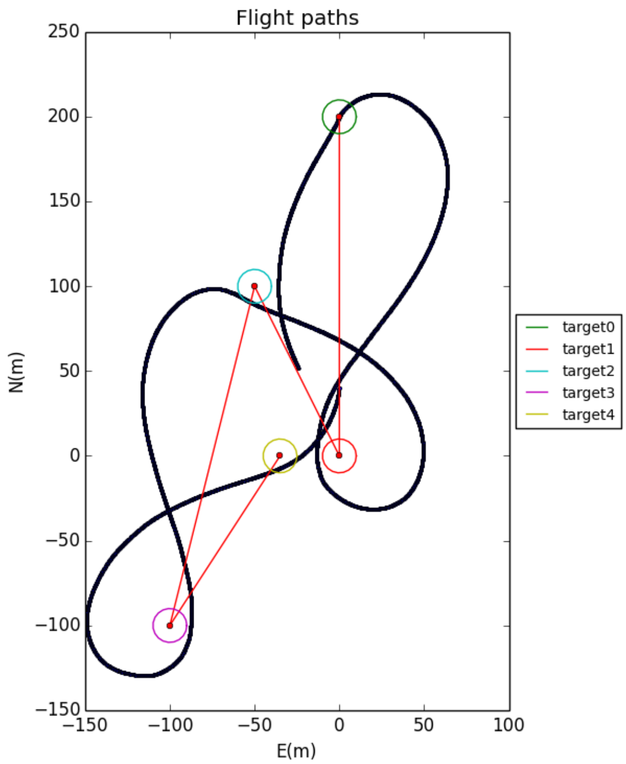

Figure 2: Bixler3: acquisition of a line and transition between lines

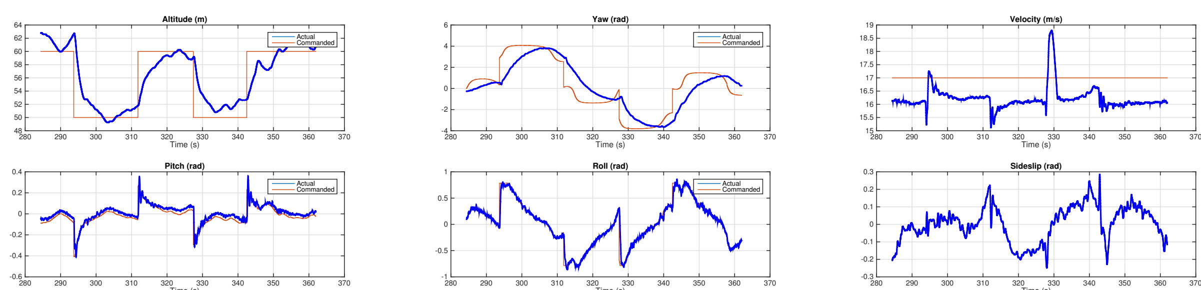

(a) Altitude and Pitch Histories **(b)** Yaw and Roll Histories **(c)** Velocity and Sideslip Histories

Figure 3: Control and State Histories for Line Switching. We see that the yaw angle is slow to change to match the desired yaw, which leads to the controller missing the desired waypoints sometimes.

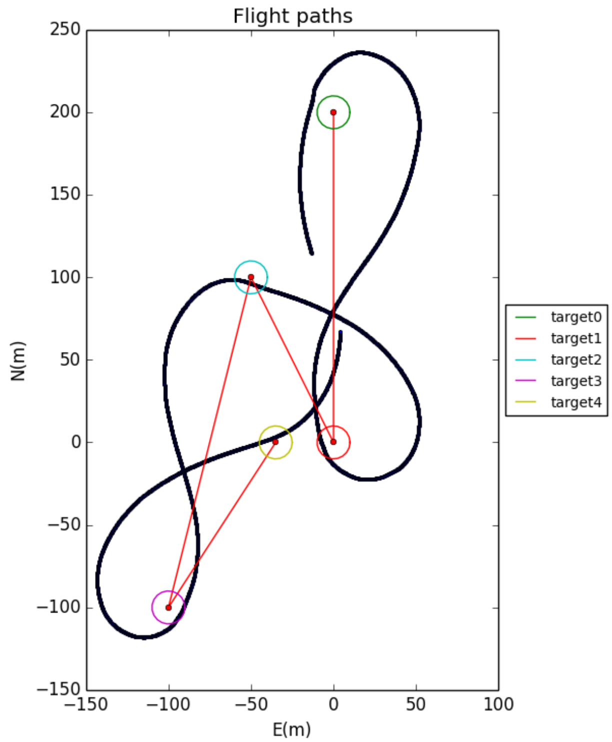

Figure 4: Bixler3: acquisition of a line and transition between lines

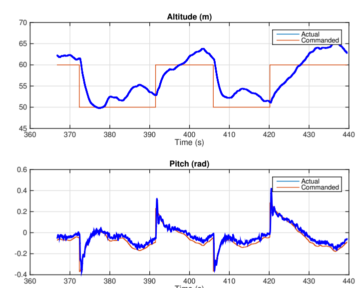

(a) Altitude and Pitch Histories

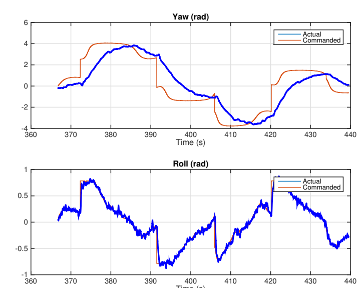

(b) Yaw and Roll Histories

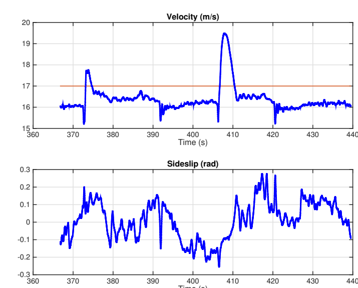

(c) Velocity and Sideslip Histories

Figure 5: Control and State Histories for Line Switching. We see that the yaw angle is slow to change to match the desired yaw, which leads to the controller missing the desired waypoints sometimes.

III Update the mission plan / strategy

Since the computational space of online planning is very limited and much is needed for the actual path following, i.e. execution of the mission, and the high level dynamic control of the plane, the mission palling should be as short - and QUICK - as possible to reduced computational effort and allocate more time for the execution of the precomputed plan.
Further to be able to switch between mission - assuming that the we could not accomplish flying through the initial set of points, we have to take re-computation-time and -power into account.

The code is working with a dynamic programming (DP) algorithm that chooses the weights based on the distances between weights points and including step-wise increasing penalties for deviation angles between the connecting lines. Very high angles are penalized dysproportionally, to be unlikely to occur, in order to lower the risk of destabilizing the plane, avoiding the requirement of high bank angles during turns.

In the following graphs, it is as well possible to see the differences between the two generated paths using a distance only based DP algorithm [fig. 6] and an optimization alogrithm taking steering angles into account. The penalization is of 10 m for each 20 degree step starting from a 80 degree.

For the simulations, as a reference the same set of waypoints for as the tested flight mission - please refer to section II. for further explanations on the test flights.

The mission compromises the waypoints:

$$North = [200., 0., 100., -100., 0.]$$
$$East = [0., 0., -50., -100., -35.]$$

The start point was arbitrarily chosen to be at [20 N, -100 E]. These coordinates are in meters, and denote an offset from the origin, that was set to [37.39958, -122.15427] latitude and longitude.

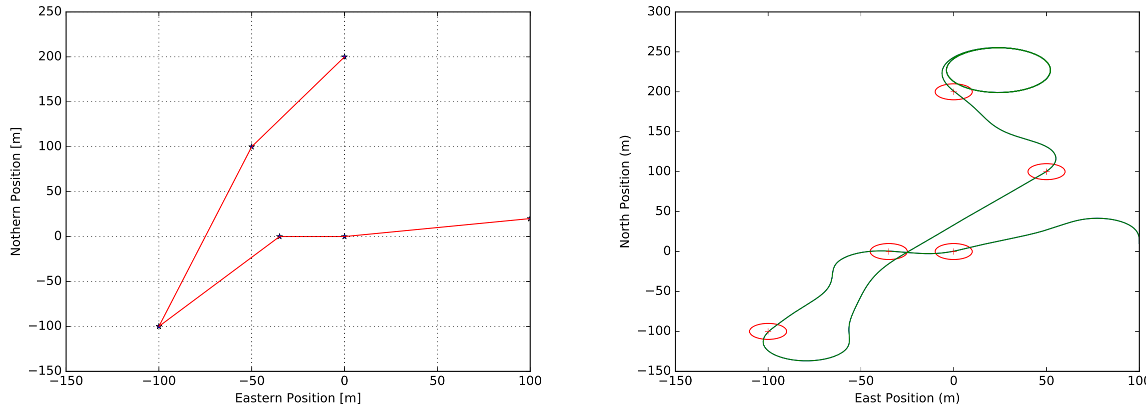

Figure 6: Path Optimization and Simulation

Clearly, as expected, the simulation with the angle penalty generates a longer path. The path looks somewhat similar to the actual path flown on the test day with this path. Obviously, it is not identical because the position of commencement is arbitrary whenever we 'switch into mission mode'.

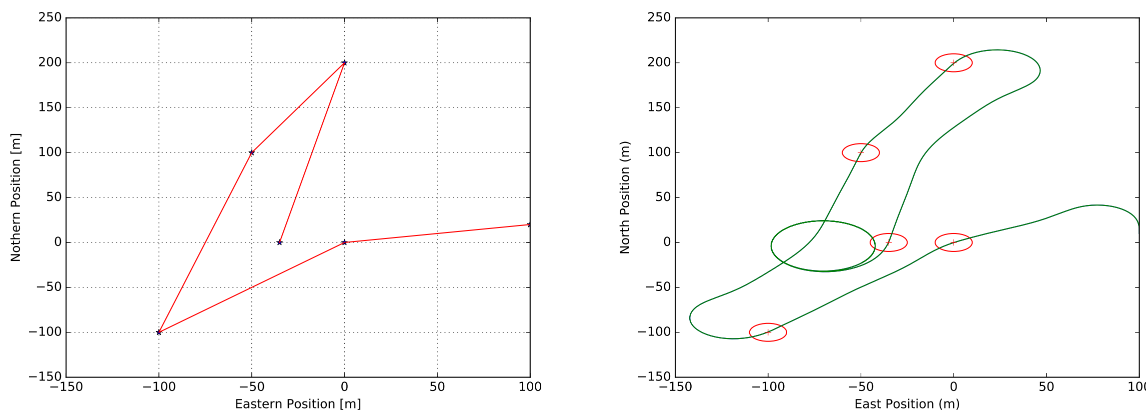

Figure 7: Path Optimization and Simulation, incl. Angle Penalization

The DP logic can genuinely be expressed by:

```
k=N
while k !=0:
        #find the optimal control step u_k* for that minimizes the cost
            function J_k
        J*_k=J(state x_N)+ sum(min(cost(state x_k, control u_k), u_k),
           k, N)
```

```
set x_k=f^(-1)(x_k, u_k*);
k-=1
```

In out case the state is the mission order and the cost or weighting function is time - i.e. distance, with or with out a angle penalty.

IV Aircraft characteristics: theory vs. experimental data

IV.1 Theoretical Data

IV.1.1 C_L, C_D, C_M

Below is a plot for theoretical C_L, C_M, C_L/C_D using XFLR5:

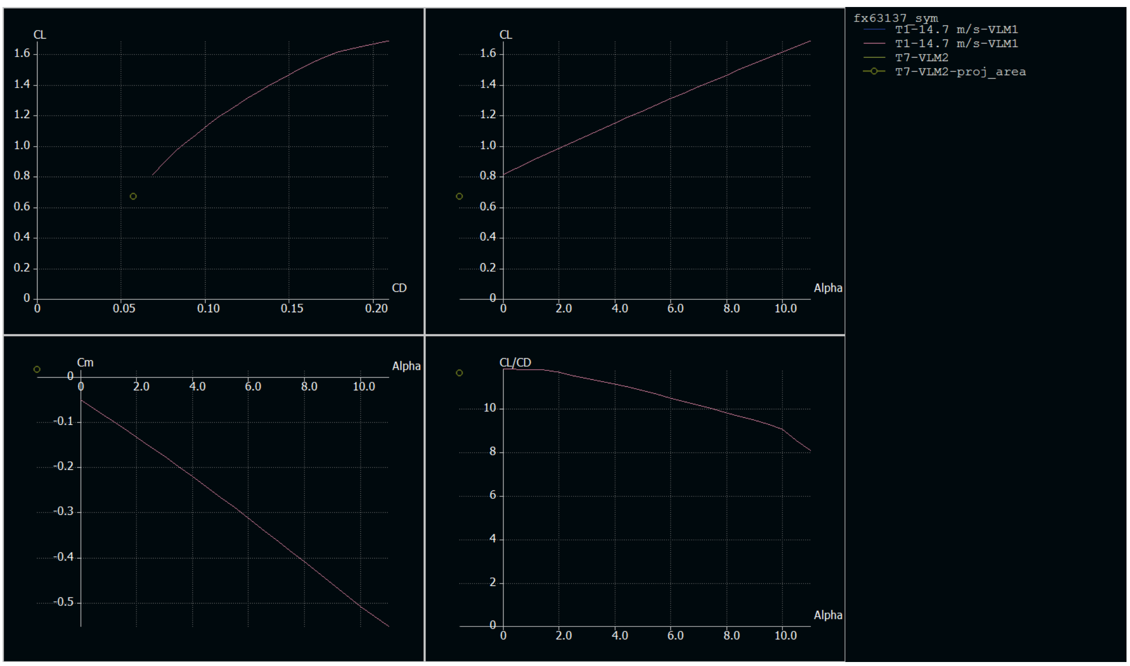

Figure 8: C_L, C_M, and C_L/C_D vs. α

IV.1.2 Fuselage Drag

Fuselage drag usually lies in the range of $30 \sim 50\%$ of the total zero-lift drag of the airplane. A more accurate estimation has to do with the fineness ratio l_B/d, where l_B is the length of the fuselage, and d is the max diameter of the fuselage. The fineness ratio for our plane is $l_B/d \approx 49/7.4 \approx 6.6$. According to the book "*Airplane Aerodynamics and Performance*" by Jan Roskam and C.T.Lan, a formula for the estimated fuselage zero-lift drag coefficient is given by:

$$C_{D_{0_f}} = R_{wf} C_{f_f} \left[1 + \frac{60}{(l_B/d)^3} + 0.0025 \left(\frac{l_B}{d} \right) \right] \frac{S_{\mathrm{wet_f}}}{S_{\mathrm{wing}}}, \tag{1}$$

where R_{wf} is the wing-fuselage interference factor shown in the figure IV.1.2; $S_{\mathrm{wet_f}}$ is the wetted area of the fuselage; C_{f_f} is the turbulent flat plane skin-friction coefficient of the fuselage given by

$$C_{f_f} = \frac{0.455}{(\log_{10} R_N)^{2.58}(1 + 0.144M^2)^{0.58}}$$

The fuselage Reynolds number is defined as:

$$R_N = \frac{\rho U l_f}{\mu}$$

During our flight test, the speed range is about $15 \sim 20$m/s, by choosing $\rho = 1.225\mathrm{kg/m^3}$, $\mu = 1.81 \times 10^{-5}$kg/m/s, the corresponding R_N value is about $497445 \sim 663260$. Since the plot below is starting from 10^6, we can make a guess that the $S_{\mathrm{wet_f}}$ value could be around 1.0. The speed of sound is about $\sqrt{1.4 \times 287 \times 298.15} = 346$m/s, and the Mach number is in the range of $0.043 \sim 0.058$. By plugging in all the values, the fuselage zero-lift drag coefficient is about $\underline{0.0081 \sim 0.0085}$. In the normal, take-off, cruise and landing angle of attack range, the fuselage drag coefficient due to lift tends to be quite negligible, so the estimated overall fuselage drag coefficient is in the range $\underline{0.0081 \sim 0.0085}$.

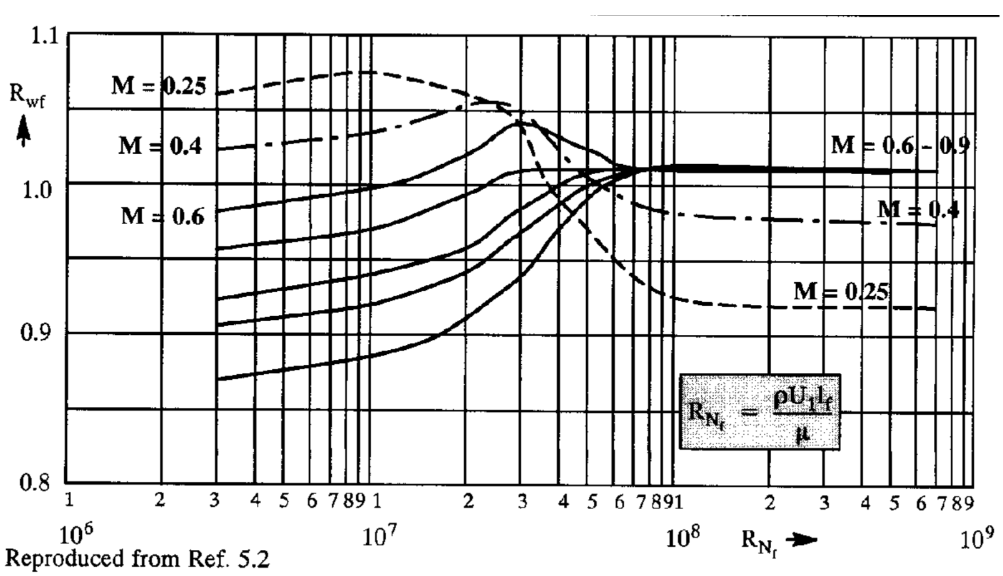

Figure 9: Wing Fuselage Interference Factor

IV.1.3 Level Flight Power

The power required for level flight is just the power to overcome drag:

$$P_{\text{req}} = DV$$

The theoretical drag coefficient without fuselage is calculated to be 0.069 using XFLR5, and from the previous part, the fuselage drag coefficient is about 0.0083 (choosing the average of the bounds), so the overall $C_d = 0.0773$. Below is a plot for required power in level flight vs. airspeed:

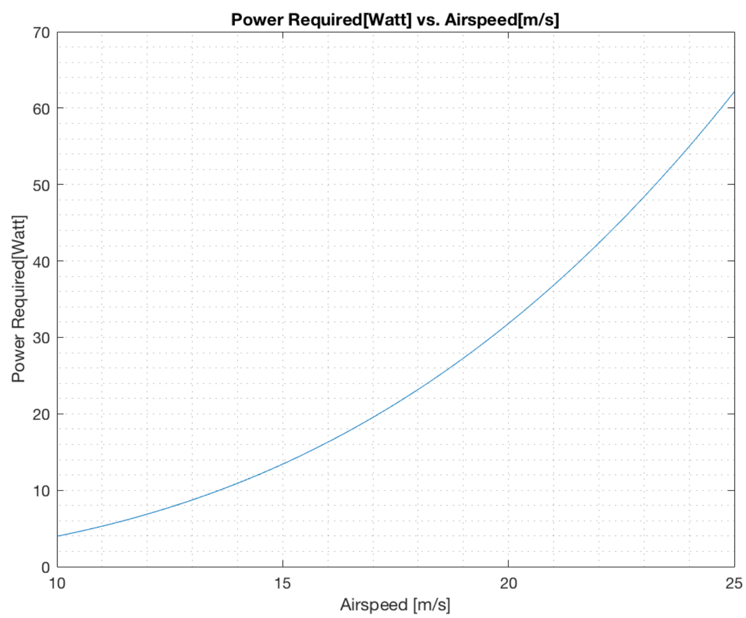

Figure 10: Power Required vs. Airspeed

IV.1.4 Power Required vs. Climb Rate

The power required for climbing is given by:

$$P_{\text{req}} = (D + mg\cos\gamma)V$$

Again, the overall drag coefficient $C_d = 0.0773$.

The Climb rate is given by:

$$\dot{h} = V\sin\gamma$$

Based on the two formulas, plots for power required vs climb rate for 4 different climb angles are given below:

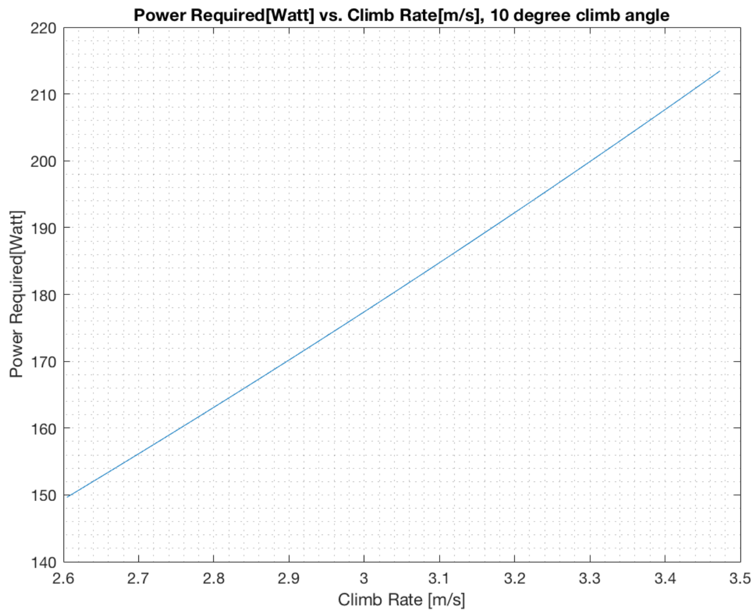

Figure 11: 10° Climb Angle

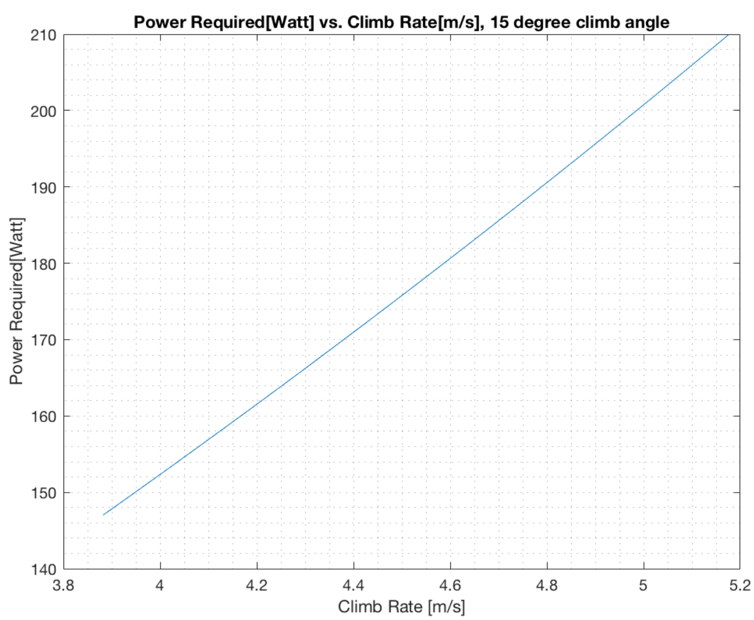

Figure 12: 15° Climb Angle

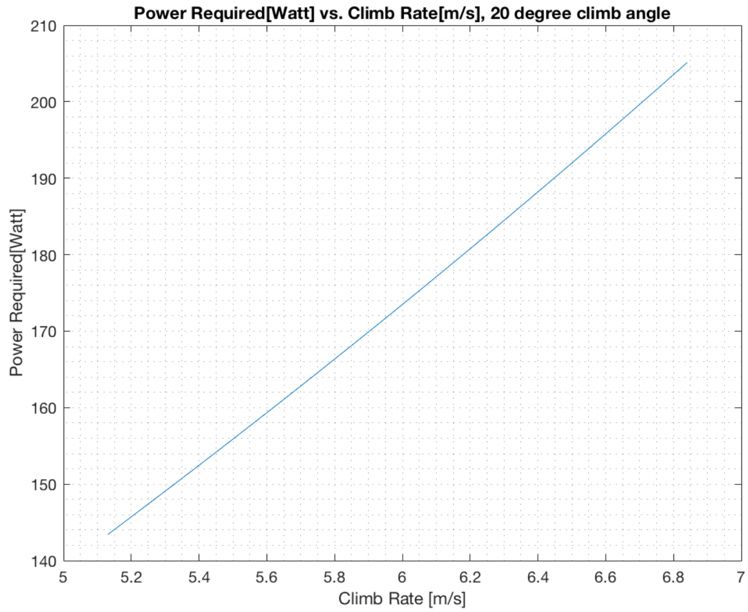

Figure 13: 20° Climb Angle

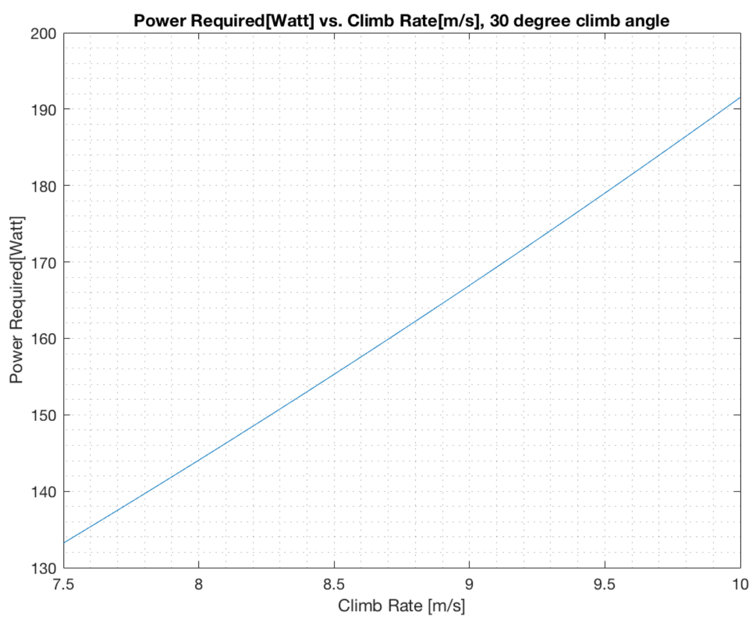

Figure 14: 30° Climb Angle

We also compute C_L from flight data, the angle of attack vs. C_L are in Fig IV.1.4 , the level flight C_L is about 0.5, which is slightly smaller than the theoretical value. But we do not have C_D, because the only flight test, we always have throttle.

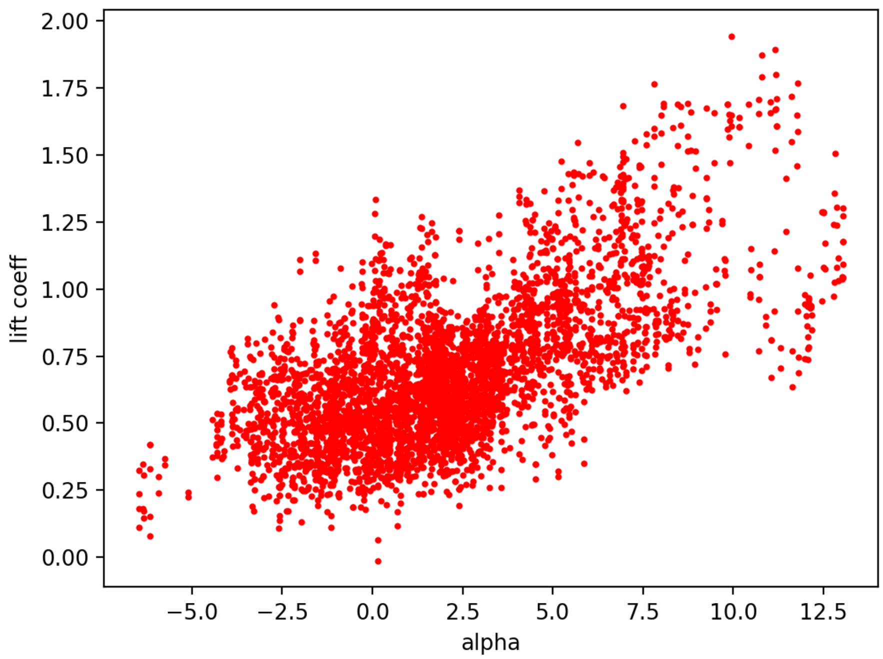

Figure 15: angle of attack vs. C_L

IV.2 Flight dynamics

The "Albatross" was flown at two trimmed speed, $V_{total} = 15.7793[m/s]$ and $V_{total} = 18.6567[m/s]$, at 81.88% and 96.69% throttle, respectively. The stability derivatives are calculated for each trimmed speed, shown in Table 1 and Table 2.

Table 1: Longitudinal Stability Derivatives

	$V_{total} = 15.7793[m/s]$	$V_{total} = 18.6567[m/s]$
C_{xu}	-0.0202	-0.0508
$C_{x\alpha}$	0.1316	0.0843
C_{zu}	-0.4727	-0.5075
C_{za}	-0.5041	-0.5002
C_{zq}	-0.5599	-0.4969
C_{ma}	-0.3771	-0.4006
C_{mq}	-4.670	-4.582

Table 2: Lateral Stability Parameters

	$V_{total} = 15.7793[m/s]$	$V_{total} = 18.6567[m/s]$
$C_{y\beta}$	-0.4850	-0.5470
C_{lb}	-0.0503	-0.0662
C_{lp}	-0.3588	-0.4459
C_{lr}	0.1334	0.1077
C_{nb}	0.1810	0.2429
C_{np}	-0.0160	-0.0172
C_{nr}	-0.0703	-0.1866

$C_{x\dot{\alpha}}$, $C_{z\dot{\alpha}}$,C_{mu},C_{yp},C_{yr} for both planes were estimated to be 0, and $C_{m\dot{\alpha}}$ was estimated as -3 as a typical value for conventional aircraft configuration. $C_{y\phi} = \frac{mg}{Sq_\infty}cos(\theta_0)$, $C_{y\psi} = \frac{mg}{Sq_\infty}sin(\theta_0)$.These stability derivatives are plugged into longitudinal and later equation of motions shown below:

$$\begin{bmatrix} \frac{mU_0}{Sq_\infty} & -\frac{c}{2U_0}C_{x\dot{\alpha}} & 0 & 0 \\ 0 & \frac{mU_0}{Sq_\infty} - \frac{c}{2U_0}C_{z\dot{\alpha}} & 0 & 0 \\ 0 & -\frac{c}{2U_0}C_{m\dot{\alpha}} & \frac{I_{yy}}{Sq_\infty c} & 0 \\ 0 & 0 & 0 & 1 \end{bmatrix} \begin{bmatrix} \dot{u} \\ \dot{\alpha} \\ \dot{q} \\ \dot{\theta} \end{bmatrix} = \begin{bmatrix} C_{xu} & C_{x\alpha} & \frac{c}{2U_0}C_{xq} & C_w cos(\theta_0) \\ C_{zu} & C_{z\alpha} & \frac{mU_0}{Sq_\infty} - \frac{c}{2U_0}C_{zq} & C_w sin(\theta_0) \\ C_{mu} & C_{m\alpha} & \frac{c}{2U_0}C_{mq} & 0 \\ 0 & 0 & 1 & 0 \end{bmatrix} \begin{bmatrix} u \\ \alpha \\ q \\ \theta \end{bmatrix}$$

$$+ \begin{bmatrix} C_{x\delta_e} & C_{x\delta_T} \\ C_{z\delta_e} & C_{z\delta_T} \\ C_{m\delta_e} & C_{m\delta_T} \\ 0 & 0 \end{bmatrix} \begin{bmatrix} \delta_e \\ \delta_T \end{bmatrix}$$

$$\begin{bmatrix} \frac{mU_0}{Sq_\infty} & 0 & 0 & 0 & 0 \\ 0 & \frac{I_{xx}}{Sq_\infty b} & -\frac{I_{xz}}{Sq_\infty b} & 0 & 0 \\ 0 & -\frac{I_{xz}}{Sq_\infty b} & \frac{I_{zz}}{Sq_\infty b} & 0 & 0 \\ 0 & 0 & 0 & 1 & 0 \\ 0 & 0 & 0 & 0 & 1 \end{bmatrix} \begin{bmatrix} \dot{\beta} \\ \dot{p} \\ \dot{r} \\ \dot{\phi} \\ \dot{\psi} \end{bmatrix} = \begin{bmatrix} C_{y\beta} & \frac{b}{2U_0}C_{yp} & \frac{b}{2U_0}C_{yr} - \frac{mU_0}{Sq_\infty} & C_{y\phi} & C_{y\psi} \\ C_{l\beta} & \frac{b}{2U_0}C_{lp} & \frac{b}{2U_0}C_{lr} & 0 & 0 \\ C_{n\beta} & \frac{b}{2U_0}C_{np} & \frac{b}{2U_0}C_{nr} & 0 & 0 \\ 0 & 1 & 0 & 0 & 0 \\ 0 & 0 & 1 & 0 & 0 \end{bmatrix} \begin{bmatrix} \beta \\ p \\ r \\ \phi \\ \psi \end{bmatrix}$$

$$+ \begin{bmatrix} C_{y\delta_a} & C_{y\delta_r} \\ C_{l\delta_a} & C_{l\delta_r} \\ C_{n\delta_a} & C_{n\delta_r} \\ 0 & 0 \\ 0 & 0 \end{bmatrix} \begin{bmatrix} \delta_a \\ \delta_r \end{bmatrix}$$

The natural frequencies and damping ratios for all the dynamic mode are calculated by linearize the equation of motion into the following form, $\dot{\vec{x}} = \mathbf{A}\vec{x} + \mathbf{B}\vec{u}$, and then calculate the eigenvalue of the matrix $\mathbf{A}$.The natural frequencies and damping ratios for all the dynamic mode for both trimmed speed are shown in Table 3 and Table 4.

Table 3: Longitudinal dynamic modes parameters

		$V_{total} = 15.7793[m/s]$	$V_{total} = 18.6567[m/s]$
$\omega_{S.P.}$	short period mode natural frequency	$4.50[\frac{rad}{\tau}]$	$5.49[\frac{rad}{\tau}]$
$\tau_{S.P.}$	short period mode time constant	1.01[s]	0.864[s]
$\zeta_{S.P.}$	short period mode damping ratio	0.22	0.211
$\omega_{phugoid}$	phugoid mode natural frequency	$0.491[\frac{rad}{\tau}]$	$0.509[\frac{rad}{\tau}]$
$\tau_{phugoid}$	phugoid mode time constant	755[s]	52.4[s]
$\zeta_{phugoid}$	phugoid mode damping ratio	2.70×10^{-3}	3.75×10^{-2}

Table 4: Lateral dynamic modes parameters

		$V_{total} = 15.7793[m/s]$	$V_{total} = 18.6567[m/s]$
$\omega_{D.R.}$	Dutch roll mode natural frequency	$7.58[\frac{rad}{\tau}]$	$10.2[\frac{rad}{\tau}]$
$\tau_{D.R.}$	Dutch roll mode time constant	1.80[s]	0.902[s]
$\zeta_{D.R.}$	Dutch roll mode damping ratio	0.0732	0.109
ω_{spiral}	spiral mode natural frequency	$0.179[\frac{rad}{\tau}]$	$0.0627[\frac{rad}{\tau}]$
τ_{spiral}	spiral mode time constant	-5.59[s]	-16.0[s]
ζ_{spiral}	spiral mode damping ratio	-1	-1
ω_{roll}	roll mode natural frequency	$22.4[\frac{rad}{\tau}]$	$32.6[\frac{rad}{\tau}]$
τ_{roll}	roll mode time constant	$0.0447[s]$	$0.0306[s]$
ζ_{roll}	roll mode damping ratio	1	1

We wasn't able to obtain trimmed flight at a lower speed since our stall speed is very high and the plane is quite hard to handle at lower speed. As shown in Table 3 and Table 4, for speed bigger than $15[m/s]$, all longitudinal modes are stable. When flying at a higher speed, we get faster Dutch roll but slower spiral divergence.

IV.3 Weight and CG statements

The designed weight for the second design iteration is 980g, the actual weight before take-off is measured to be 940g. The detailed drag build-up is shown in Table 5.

Table 5: Weight break-down [g]

Total preflight mass	940
Fuselage	199
Battery	177
Wing + Aileron + Servos	106
Wing box	99
Electronics	58
Tail assembly + rod	65

The CG is made to be at approximately quarter chord of wing, which is where the wing spar is located. The CG is checked before each flight.

IV.4 Design and Manufacturing

Our second iteration was on the layout and design mentioned and explained on PS 2. The gaol was to set a wing up for a lower total weight and to reduce instabilty of the sprial mode most notably without destabilizing the others. Compared to our first design iteration of the plane with 1.5 kg, the second was of 980 g, which is the estimated minimum weigth require to bare all the electronics added to a foam wing, tail, basswood ailerons and rudder and the fuselage, see Table 5 for the weight breakdown.

The wing is designed is depicted below (Fig 16) and the geometric parameters are gathered in [Table 6].

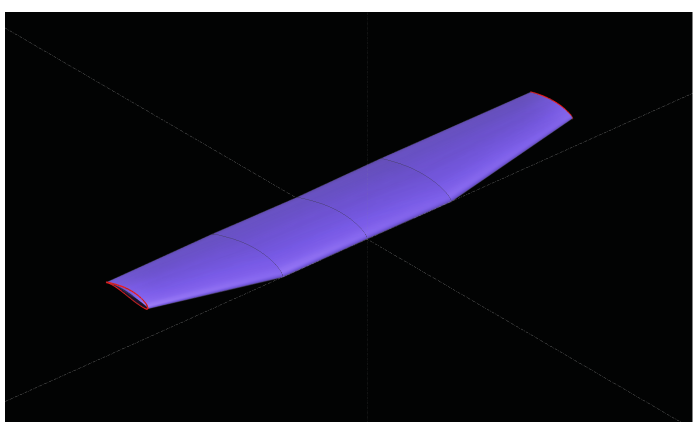

Figure 16: Wing Design, Iteration 2

Table 6: Geometric Parameters

wing span	.71m
Area	.08 m^2
Mean Geo. Chord	.12m
AR	6.00
TR	1.69

We were designing a dihedral of 10 degrees, which was impossible to manufacture, the highest dihedral feasible was of 8.5 degrees.

The manufacturing was similar to our the one of our first plane. The main differences and improvements were:

1. The Spar. The carbon rod was this time continuous through the middle section. Also did we reinforce the carbon spar junctions for at the connection between middle in the side parts on both sides, by including an internal piece of plywood in the hollow center of the rod.

2. The tail mount. Our first planes mount was very loose and unstable. Hence this time we prevented any rotational movements by adding a separate spare on the side that slides into a specific slot in the fuselage.

3. Ailerons. We decided to use basswood instead of foam for the manufacturing of the ailerons, in order to reduce the effects of torsion moments during turns.

Unfortunately we broke some of our planes' parts during out initial flights, when testing the line following and altitude hold. We manufactured them and put the plane back together. Ultimately, on our last test flight, we had issues at take off and nosedived pretty quickly after a few meters due to a high roll angles that could not recovered automatically in this really short period of time. We assume that small imperfections in the wing manufacturing caused the high bank-angle tendency.

Consequentially, we are going to redesign the wing in a much simpler way such that these manufacturing artifacts do not impede the success of our total operating system. A flat wing design will do the job.

The wing that was designed as third and last iteration is depicted below (Fig 17) and its geometric parameters are listed in [Table 7].

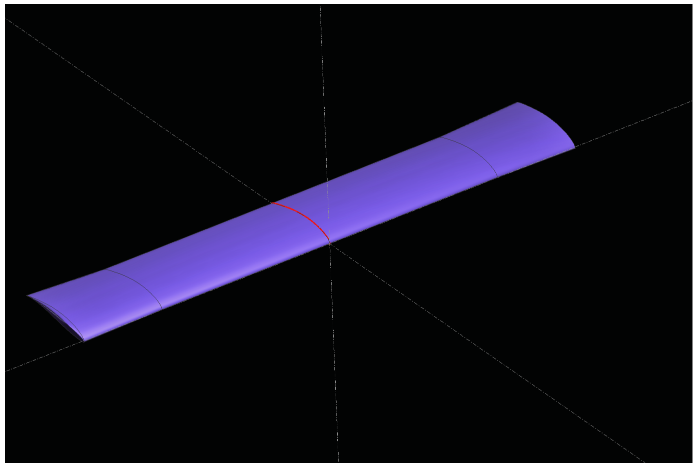

Figure 17: Wing Design, Iteration 3

Table 7: Geometric Parameters

wing span	.73m
Area	.09 m^2
Mean Geo. Chord	.12m
AR	6.00
TR	1.0

It does not have any offset or dihedral but a sweep angle of -4 degrees at the tips.

V Minimum turning radius

This section shows the experimental result Albatross' minimum turning angle. For our plane is not roll stable, so we do it conservatively, Figs 18 show the turning trajectory, the turning radius is about 15m

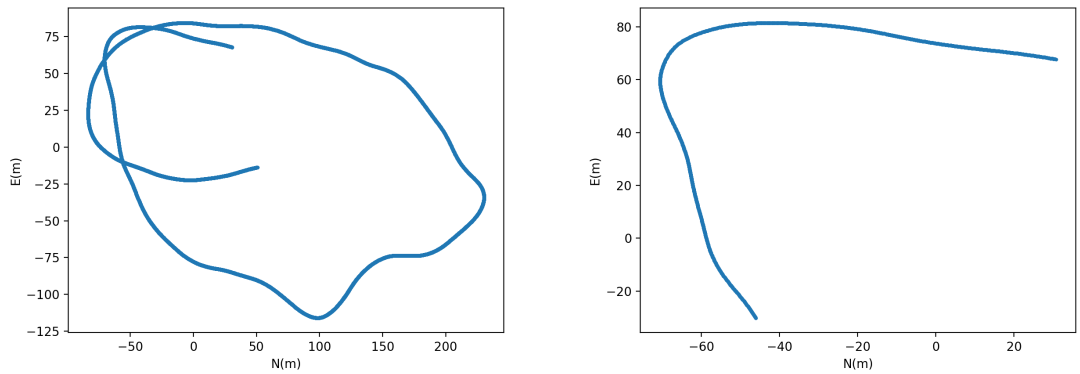

Figure 18: Turing path

Figs 19 show the bank angle and channel input, the maximum of bank angle is almost 90 degrees

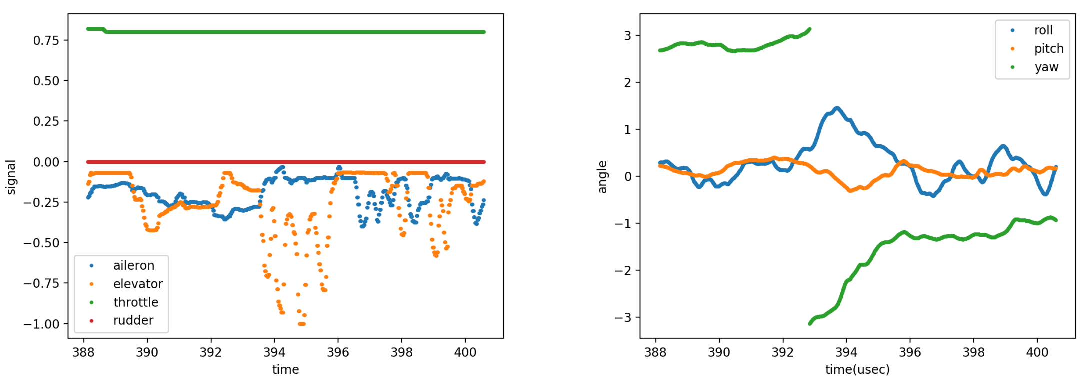

Figure 19: Singnal and bank angle

Figs 18 show the C_L and lift of turning, our plane is about 1Kg, this turn is a 1.5G - 2G turn

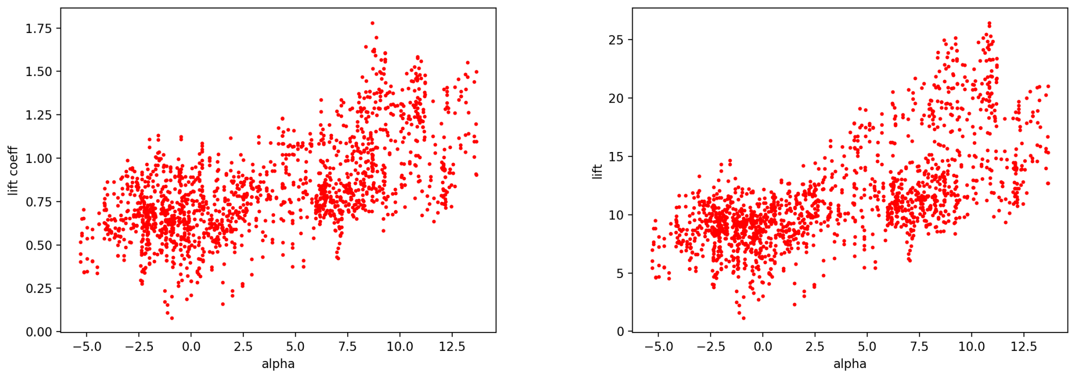

Figure 20: lift and C_L during turning

VI Goals and Plan of Action

Currently, we have had one line following and line switching mostly successful on the Bixler. The Albatross model was only successfully flown once, and the control algorithm need to be tested on the Albatross model before the fly-off. The detailed task table and gantt chart are shown in Fig.21 and Fig.22 respectively.

	Task Name	Start Date	End Date	Duration	Predecessors	% Complete	Status
1	**Construction**	**06/05/17**	**06/08/17**	**4d**		**17%**	**In Progress**
2	rebuild airplane	06/05/17	06/05/17	1d		50%	In Progress
3	build back-up parts	06/07/17	06/08/17	2d		0%	Not Started
4	**Flight test**	**06/04/17**	**06/09/17**	**6d**		**8%**	**In Progress**
5	One line following and switching lines on Bixler	06/04/17	06/04/17	1d		100%	Completed
6	Incorporate path optimization on Bixler	06/06/17	06/07/17	2d		0%	In Progress
7	Autonomous stabilization mode test on our airplane	06/05/17	06/07/17	3d		0%	Not Started
8	One line following on our airplane	06/07/17	06/08/17	2d		0%	Not Started
9	Switching lines on our airplane	06/07/17	06/08/17	2d		0%	Not Started
10	Incorporate path optimization on our plane	06/07/17	06/09/17	3d		0%	Not Started

Figure 21: Task table

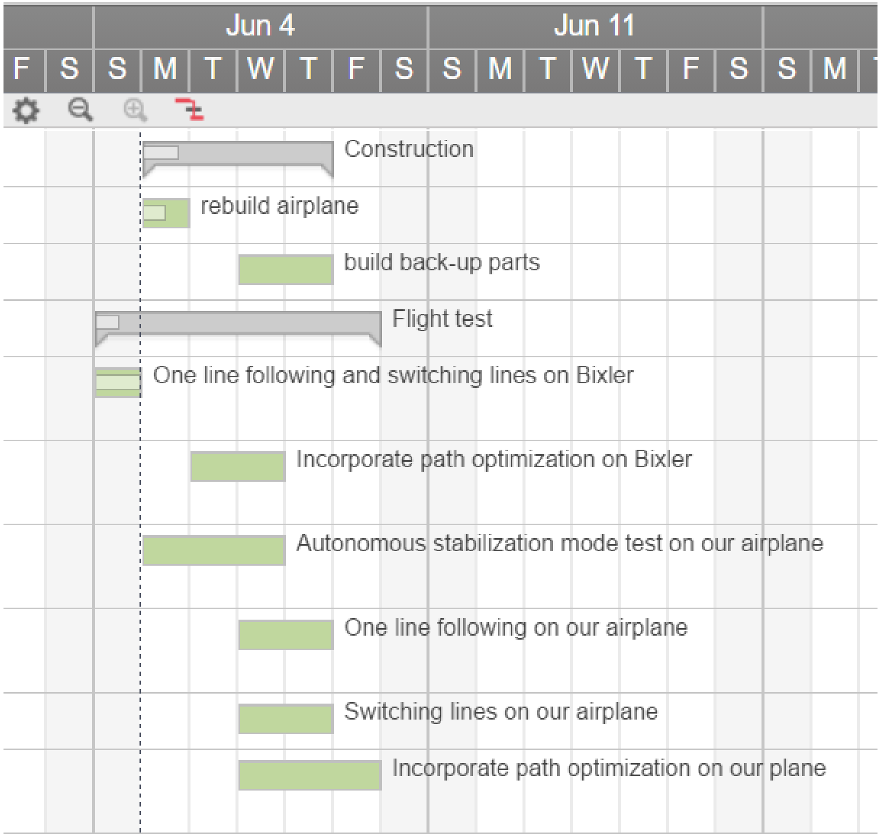

Figure 22: Gantt chart

Comparing to the goals set in problem set 2, we were able to finish building our second prototype and perform flight test; however, we didn't get to try our control algorithm on our airplane, thus we weren't able to tune the control gains for our specific aircraft configurations as we wished, because we crashed our aircraft more than expected. We hope to flight test the mission on our aircraft in the next following days before fly-off.

Appendix

Table 8: Writing Contribution

I.	Apoorva Sharma
II.	Zhengyu Huang, Apoorva Sharma
III.	Victoria M. Dax
IV. 1.	Zhe Zhang
IV. 2.	Miao Zhang
IV. 3.	Miao Zhang
IV. 4.	Victoria M. Dax
V.	Zhengyu Huang
VI.	Miao Zhang

References

[1] John H. Blakelock, *Automatic Control of Aircraft and Missile* A Wiley-Interscience publication: John Wiley & Sons, 1991.

[2] Randal W. Beard, Timothy W. McLain, *Small Unmanned Aircraft: Theory and Practice.* Princeton University Press, 2012.